Developmental Biology 409 (2016) 297–309

Contents lists available at ScienceDirect

Developmental Biology

journal homepage: www.elsevier.com/locate/developmentalbiology

Evolution of Developmental Control Mechanisms

Comprehensive analysis of Hox gene expression in the amphipod crustacean *Parhyale hawaiensis*

Julia M. Serano [a], Arnaud Martin [a], Danielle M. Liubicich [b,c], Erin Jarvis [b], Heather S. Bruce [a], Konnor La [b], William E. Browne [d], Jane Grimwood [e], Nipam H. Patel [a,b,*]

[a] Department of Molecular Cell Biology, University of California, Berkeley, CA 94720-3200, USA
[b] Department of Integrative Biology, University of California, Berkeley, CA 94720-3140, USA
[c] Los Medanos College, 2700 East Leland Rd., Pittsburg, CA 94565, USA
[d] Department of Biology, University of Miami, 1301 Memorial Drive, Coral Gables, FL 33146, USA
[e] HudsonAlpha Genome Sequencing Center, 601 Genome Way, Huntsville, AL 35806, USA

ARTICLE INFO

Article history:
Received 6 September 2015
Received in revised form
25 October 2015
Accepted 25 October 2015
Available online 10 November 2015

ABSTRACT

Hox genes play crucial roles in establishing regional identity along the anterior–posterior axis in bilaterian animals, and have been implicated in generating morphological diversity throughout evolution. Here we report the identification, expression, and initial genomic characterization of the complete set of Hox genes from the amphipod crustacean *Parhyale hawaiensis*. *Parhyale* is an emerging model system that is amenable to experimental manipulations and evolutionary comparisons among the arthropods. Our analyses indicate that the *Parhyale* genome contains a single copy of each canonical Hox gene with the exception of *fushi tarazu*, and preliminary mapping suggests that at least some of these genes are clustered together in the genome. With few exceptions, *Parhyale* Hox genes exhibit both temporal and spatial colinearity, and expression boundaries correlate with morphological differences between segments and their associated appendages. This work represents the most comprehensive analysis of Hox gene expression in a crustacean to date, and provides a foundation for functional studies aimed at elucidating the role of Hox genes in arthropod development and evolution.

1. Introduction

Few developmental gene families have been studied as extensively as the Hox genes, which encode homeodomain-containing transcription factors that determine regional identity along the anterior–posterior (AP) axis in bilaterian animals (Pourquié, 2009). Hox genes are typically organized within the genome in conserved clusters that display spatial colinearity—that is, their position along the chromosome correlates with the positions of their expression domains along the AP axis. Perturbation of Hox gene expression is associated with homeotic transformations, wherein body parts in one region of an animal are transformed to more closely resemble those of another region. Given the importance of Hox genes in establishing regional and segmental identity, it is not surprising that numerous lines of molecular, genetic, and developmental evidence have implicated Hox genes in generating morphological diversity during animal evolution.

Arthropods have proven to be especially well suited for studying the contribution of Hox genes to evolutionary changes in morphology (reviewed in Angelini and Kaufman, 2005; Hughes and Kaufman, 2002a). Arthropods have clearly segmented body plans, and each segment typically possesses a single, often unique, pair of appendages and other characteristics that provide useful markers for segmental identity. Furthermore, homologous segments between related arthropod species often display significant differences in appendage morphology. This allows one to ask questions about how differences in Hox gene expression, and the response of downstream target genes, generate segmental and appendage diversity, both within a single organism as well as between different species. Analyses of Hox gene expression in various arthropod lineages have led to a number of intriguing hypotheses linking observed shifts in Hox expression domains to specific morphological differences (Abzhanov and Kaufman, 1999a, 2000a; Averof and Patel, 1997; Hughes and Kaufman, 2002a; Hughes et al., 2004; Mahfooz et al., 2004; Peterson et al., 1999; Rogers et al., 1997). As a member of a major lineage, Malacostraca, within the Pancrustacean clade (Misof et al., 2014; Regier et al., 2010), which comprises all crustaceans and hexapods, *Parhyale* is well positioned as both an

* Corresponding author at: Department of Molecular Cell Biology, University of California, Berkeley, CA 94720-3200, USA.
E-mail address: nipam@berkeley.edu (N.H. Patel).

http://dx.doi.org/10.1016/j.ydbio.2015.10.029
0012-1606/

outgroup of insects and as a reference crustacean for evolutionary developmental studies of the diversity of arthropod *bauplans* (Rehm et al., 2009a).

The *Parhyale* body plan is fairly typical of the crustacean order Amphipoda. From anterior to posterior, the head segments include a pre-antennal segment (which lacks paired appendages), the first antennal (An1), second antennal (An2), mandibular (Mn), first maxillary (Mx1), and second maxillary (Mx2) segments. The thorax is comprised of eight segments, T1 through T8. The T1 appendages are maxillipeds, which, along with the mandible and the two maxillae, facilitate feeding. The gnathopods on T2 and T3 have a distinctive distal claw; the T3 claw grows especially large in adult males. Segments T4 through T8 contain walking legs. The walking legs on T4 and T5 are oriented anteriorly, while those on T6 through T8 are larger, have thicker bristles, and are oriented posteriorly (the name of the order, "Amphipoda", derives from having these two distinctly different walking legs. The abdomen consists of six segments, A1 through A6, each bearing a pair of biramous appendages. The pleopods (swimmerets) of A1 through A3 are indistinguishable from one another, whereas the uropods (anchor legs) of A4 through A6 significantly decrease in size from anterior-to-posterior.

As a first step toward a comprehensive analysis of Hox gene function and evolution in crustaceans, we have cloned and examined the expression patterns for the entire *Parhyale* Hox gene suite. We have identified a single copy of each canonical Hox gene with the exception of *fushi tarazu (ftz)*. Our preliminary BAC data indicate that many, if not all, *Parhyale* Hox genes are clustered in the genome. Expression analyses demonstrate that, with a couple of exceptions, they exhibit both temporal and spatial colinearity. Many of the Hox expression boundaries coincide with obvious morphological differences between appendage types and/or tagmata. The work presented here forms the foundation for future studies aimed at examining the role that Hox genes play in crustacean development and arthropod evolution.

2. Materials and methods

2.1. Cloning Parhyale Hox genes

Parhyale embryos of mixed ages were collected to make cDNA as previously described (Price and Patel, 2008). We used a variety of degenerate PCR primers targeting either the homeodomain or hexapaptide regions of Hox genes. The forward primers we initially used were 5'-YTIGARYTNGARAARGARTT-3', 5'-ACITAYACNCGNTAYCARAC-3', 5'-ACICGITAYCARACNYTNGA-3', 5'-CARACIYTIGARYTNGARAA-3', 5'-ATITAYCCNTGGATGMGN-3', 5'-ATHTAYCCNTGGATGGCN-3', 5'-ATHTAYCCNTGGATGAAR-3', 5'-CARATHTAYCCNTGGATG-3', and reverse primers were 5'-CKRTTYTGRAACCANATYTT-3' and 5'-CATWCKWCKRTTYTGRAACCA-3'. The method we found to be most useful for isolating the broadest possible range of Hox genes involved creating a series of less-degenerate primers targeting the highly conserved LELEKEF and KIWFQNR motifs in the Hox homeodomain. Four LELEKEF forward primers (5'-YTNGARYTNGARAAAGAATT-3', 5'-YTNGARYTNGARAAAGAGTT-3', 5'-YTNGARYTNGARAAGGAATT-3', 5'-YTNGARYTNGARAAGGAGTT-3') were used in every possible combination with four KIWFNQR reverse primers (5'-CKRTTYTGRAACCASATCTT-3', 5'-CKRTTYTGRAACCASATTTT-3', 5'-CKRTTYTGRAACCAWATCTT-3', 5'-CKRTTYTGRAACCAWATTTT-3'). Because the 3′-most nucleotides of each primer are not degenerate, PCR amplifications tended to be specific for certain Hox genes but not others—this circumvented the problem of repeatedly re-isolating the same few (perhaps most highly abundant) Hox genes. Each primer was used at a final concentration of 5 μM in 50 μl PCR reactions that included 2.5 units of Taq DNA Polymerase (New England BioLabs), 1 × ThermoPol buffer (New England BioLabs), 1.5 mM $MgCl_2$, 0.2 mM dNTPs, and embryonic cDNA. Forty cycles of amplification were carried out at a melting temperature of 94 °C, a "step-down" annealing temperature starting at 63 °C and decreasing 1 °C per cycle to 52 °C, and an extension temperature of 72 °C. PCR products were run on a 2% agarose gel, 120 nt fragments were isolated *via* low melting point agarose and directly cloned into pBluescript II (Stratagene). Miniprep DNA was directly sequenced. In some case, colonies were pre-screened by PCR using oligos specific for previously isolated *Parhyale* Hox genes in order to identify those clones that would most likely represent novel Hox genes.

5′ and 3′ flanking sequences for each identified Hox gene were isolated using the GeneRacer (Invitrogen) and/or GenomeWalker (Clontech Laboratories) kits. When possible, primers were designed to the 5′- and 3′most sequences of the untranslated regions (UTRs) for each Hox gene and used to PCR-amplify full-length cDNAs. Accession numbers for *Parhyale* Hox cDNA sequences are as follows: *labial*, JQ952576; *proboscipedia*, JQ952587; Hox3, JQ845948; *Deformed*, JQ952571; *Sex comb reduced*, JQ952579; *Antennapedia variant I*, JQ952581; *Antennapedia variant II*, JQ952582; *Ultrabithorax isoform I*, FJ628448; *Ultrabithorax isoform II*, FJ628449; *abdominal-A* isoform I, Q952572; *abdominal-A* isoform II, JQ952573; *Abdominal-B* isoform I, JQ952574; *Abdominal-B* isoform II, JQ952575.

2.2. BAC library screening

Parhyale BAC screening using radiolabelled Hox probes was carried out according to (Parchem et al., 2010). Inverse PCR was employed to generate sequence data for the 5′ and 3′ ends for many of the Hox-positive BAC clones. In some cases, inverse PCR-derived probes were used to re-screen the *Parhyale* BAC library. Miniprep DNA from 96 unique Hox-positive BACs was spotted onto "dot-blots," and each blot was hybridized to probes derived either from portions of Hox cDNAs and from the 5′ and 3′ ends of specific BAC clones. This dot-blot data was used to construct a rough map of the *Parhyale* Hox complex(es), and this map was refined and verified using BAC sequencing data. Accession numbers for the *Parhyale* Hox BAC sequences are as follows: PA31-H15, KR869963; PA24-C06, KR869964; PA93-L04, KR869965; PA264-B19, KR869966; PA179-K23, KR869967; PA40-O15, KR869968; PA81-D11, KR869969; PA272-M04, KR869970; PA92-D22, KR869971; PA221-A05, KR869972; PA284-I07, KR869973; PA76-H18, KR869974; PA120-H17, KR869975; PA268-E13, KR869976; PA222-D11, KR869977.

2.3. In situ hybridization and imaging

Embryo dissection, fixation, and *in situ* hybridization were carried out according to Rehm et al. (2009b,2009c) and Vargas-Vila et al. (2010). Images were analyzed on a Zeiss Axiophot microscope, captured in color with a Diagnostic Instruments Spot Camera, and figures assembled using Adobe Photoshop. False-color overlays of *in situ* hybridization images were carried out as follows: The DAPI signal was photographed and shifted to cyan by adjusting the hue to −35. A bright field image of the histochemical staining (from the BCIP/NBT/alkaline phosphatase reaction; Roche) was inverted, and the blue and green channels were eliminated so that the staining appears red. In double-staining experiments, the fluorescent signal from the Fast Red (Roche) product was photographed and shifted to yellow by adjusting the hue to +50. The "screen" command was applied to the red, yellow and DAPI images to allow all signals to be visualized simultaneously.

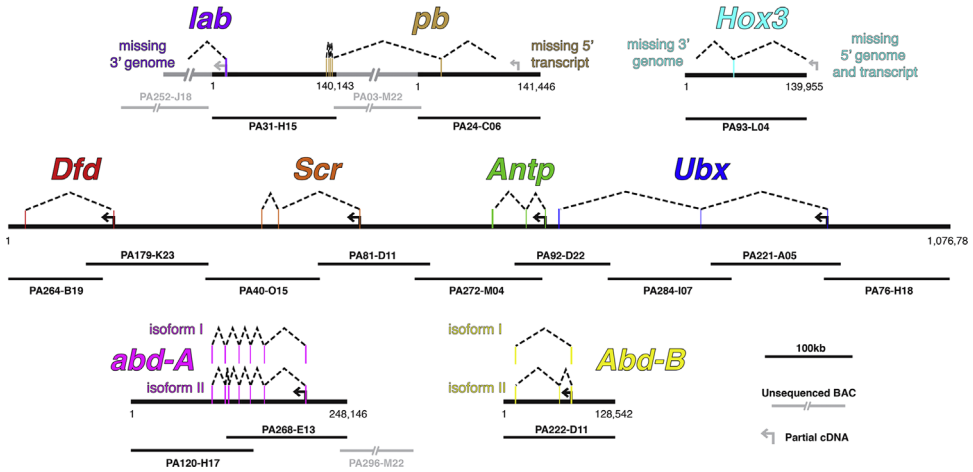

Fig. 1. Genomic organization of Parhyale Hox genes. The nine Parhyale Hox genes, along with the putative position of their respective promoters and intron/exon structure, are shown in relation to 18 BACs. Each BAC ranges from 100–150 kb in size. Based on our genomic mapping, two sets of genes, Ubx-Antp-Scr-Dfd and pb-lab, are contiguous with one another. Our data is inconclusive as to whether the remaining three Hox genes (Abd-B, abd-A and Hox3) are linked to one another or to the aforementioned Hox genes.

2.4. Immunohistochemistry

Antibody staining was carried out following previously published protocols (Liubicich et al., 2009; Patel, 1994; Rehm et al., 2009d). For detection of *Parhyale* Ubx we used a rat polyclonal antibody at a 1:4000-6000 dilution (Liubicich et al., 2009). Antp was detected using the previously described crossreactive mouse monoclonals 4C3 and 8C11 at dilutions of 1:30–1:50 (Condie et al., 1991; Hayward et al., 1995; Saenko et al., 2011); the two monoclonals displayed identical patterns in *Parhyale* embryos. Embryos were imaged using either an LSM 700 or LSM 780 (Zeiss) confocal microscope, and processed using Volocity software (Perkin-Elmer). For all *in situ* and immunohistochemical embryo preparations, all images are ventral views unless stated otherwise.

2.5. CRISPR/Cas9-mediated homologous recombination

We synthesized a sgRNA targeting the codons 7–14 of *Antp* following the procedure of (Bassett and Liu, 2014). To generate a donor plasmid for homologous recombination around the cleavage site, we cloned a genomic DNA fragment of 2.1 kb approximately centered on the *Antp* start codon (forward primer: 5′-CCCGAACTGTAAAAGGCAAA ; reverse primer: 5′-TGCTGGGCAAAAGAAAAACT-3′) into the pGEM-T vector (Promega). A linear fragment was created by inverse PCR and Gibson Assembly used to integrate an *EGFP* sequence followed by the T2A ribosome skipping peptide signal (Diao and White, 2012) to the 5′ coding region of *Antp*, generating a *pHR_EGFP-T2A-Antp* donor for fluorescent tagging of *Antp*-expressing cells. Using modified oligonucleotides for fragment amplification, we also altered the PAM sequence in the donor plasmid to avoid secondary cleavage after successful homologous repair. We injected embryos at the one-cell stage with 40–60 picoliters of an injection mix containing the *Antp* sgRNA (200 ng/μL), the *AntpHR1_EGFP-T2A_AntpHR2* donor plasmid (200 ng/μL), a recombinant Cas9 protein (333 ng/μL, PNABio), and Phenol Red (0.05% final concentration). Embryos were screened for eGFP signal with a Lumar.V12 stereomicroscope (Zeiss) and imaged with a LSM780 confocal microscope (Zeiss).

3. Results

3.1. Isolation and genomic mapping of Parhyale Hox genes

We used a comprehensive degenerate PCR strategy to identify the entire set of *Parhyale* Hox genes. This approach resulted in the isolation of the homeobox sequences from all of the canonical Hox genes with the exception of *ftz* (see Supplemental Fig. 1). In subsequent cloning, we were able to isolate full-length cDNAs for *labial (lab), Deformed (Dfd), Ultrabithorax (Ubx), abdominal-A (abd-A)* and *Abdominal-B (Abd-B),* and the entire open reading frame for *Sex combs reduced (Scr)*. For *proboscipedia (pb)* and *Antennapedia (Antp),* we obtained cDNA sequence 5′ and 3′ to the homeobox, but not a full-length cDNA, and for *Hox3* we only isolated sequence 3′ to the homeobox. Our analyses suggest that *Parhyale* has a single copy of each of these Hox genes. Multiple alternatively spliced variants for *Ubx* (Liubicich et al., 2009), *abd-A*, and *Abd-B* were identified; for each gene, these alternatively spliced versions are referred to as *isoform-1* and *isoform-2*. For *Antp*, two classes of cDNA differing from one another at three distinct polymorphic regions within the coding region were identified. Since these polymorphic variants (alleles) encode slightly different proteins, we refer to them here as *Antp variant I* and *Antp variant II*. We also found that a subset of transcripts transcribed from the *Ubx* promoter(s) are spliced to exons from the *Antp* transcription unit, indicating that transcriptional read-through occurs between the two genes. Similar *Ubx-Antp* read-through transcripts have been reported for five other crustaceans, two myriapods, and an onychophoran (an outgroup to arthropods), suggesting that this may be a relatively ancient feature of arthropod Hox complexes (Brena et al., 2005; Janssen and Budd, 2010; Shiga et al., 2006).

To determine whether *Parhyale* Hox genes are organized into clusters, we screened a *Parhyale* BAC library (Parchem et al., 2010) using probes specific for each Hox gene. Sequences from the ends of each positive BAC clone were also used as templates for probes to both re-screen the BAC library and to map individual BACs in relation to one another. Once sequenced, we were able to confirm our BAC map and precisely define the overlap between BACs (Fig. 1). As shown in Fig. 1, one set of BACs together span four linked Hox genes (5′-*Ubx, Antp, Scr, Dfd*-3′) and a second spans two linked Hox genes (5′-*pb, lab*-3′). In both cases, the Hox genes are organized in a linear, 5′-to-3′ orientation consistent with what has been reported for vertebrate and other Hox clusters. BAC clones corresponding to the three remaining Hox genes *(Abd-B, abd-A* and *Hox3)* were also isolated, but we were unable to determine whether they are located near or adjacent to each other and/or the aforementioned Hox mini-clusters. Given that *Parhyale* has a relatively large genome size (Parchem et al., 2010), additional genome data will be required to determine whether all nine Hox

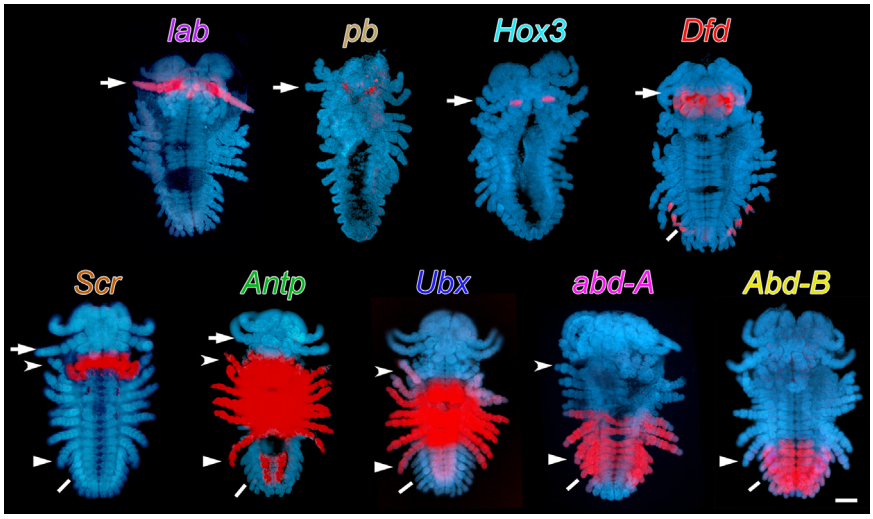

Fig. 2. *Parhyale* Hox gene expression. Anterior is at top. *In situ* hybridization patterns for each Hox gene in ventral views of stage 22–24 embryos. Nuclei are stained with DAPI (blue) and the corresponding Hox *in situ* pattern is in red. Specific appendages are indicated by the following symbols, arrow: antennae 2; arrowhead: T2 leg; triangle: T8 leg; bar: A3 pleopod. Scale bar 100 μm. (For interpretation of the references to color in this figure legend, the reader is referred to the web version of this article.)

genes are organized within a single, large genomic cluster.

3.2. Hox gene expression during Parhyale embryogenesis

To gain insight into the potential function of *Parhyale* Hox genes in patterning and segmental identity, we examined their embryonic expression patterns *via in situ* hybridization. We started by examining the expression of all nine Hox genes at stage 22–24, a time when all segments are clearly visible and the different appendage types have taken on their unique morphologies (Fig. 2). Each Hox gene is expressed in a unique, but often overlapping, domain along the anterior–posterior (AP) axis. Hox genes generally display spatial colinearity, with the relative domains of expression along the embryonic A–P axis aligned to the relative genomic position of the individual genes within the complex. This spatial colinearity appears conserved in *Parhyale,* at least within the limits of our preliminary data on clustering: *lab, pb, Hox3* and *Dfd* expression is restricted to head segments, *Scr* and *Antp* span the head and thoracic segments, *Ubx* is expressed predominantly in the thorax, *abd-A* spans the thoracic and abdominal segments, and *Abd-B* is restricted to the abdomen (Fig. 2).

For each Hox gene, we then analyzed its expression through all stages of development (see below). The stages of *Parhyale* embryogenesis discussed here have been previously described (Browne et al., 2005). The germband forms shortly after gastrulation, when most of the cells in the embryo migrate to the anterior end and condense to form the early germ disc. Over time, ectodermal cells organize themselves into a germband composed of an orderly grid beginning in the posterior part of the head. We refer to the first row that forms as “row 1,” and the row that eventually forms just anterior to it as “row 0.” Rows 0 and 1 together appear to comprise the future parasegment 1, which ultimately gives rise to the posterior of the Mn and the anterior of Mx1. Each transverse cell row that forms posterior to row 1 will give rise to a single parasegment, and is thus termed a parasegmental precursor row (PSPR). In succession, PSPR 2 (the cell row immediately posterior to row 1) through PSPR 16 (which gives rise to the posterior-most parasegment) undergo two rounds of mitotic division that proceed in waves from medial to lateral and from anterior to posterior. The first mitotic wave (FMW) results in two rows of progeny cells: a/b and c/d. These cells divide again during the second mitotic wave (SMW) to yield four rows of cells (a, b, c, d).

We also employed two additional markers to assist in assigning the precise boundaries of Hox gene expression relative to segmentation and appendage development: *engrailed* (*en*) and *Distal-less* (*Dll*). *Engrailed* expression can be detected in the “a” cell of each parasegment (Browne et al., 2005; Patel et al., 1989). As in other arthropods, *engrailed* expression marks the anterior boundary of each parasegment and the posterior boundary of each morphological segment. Cells anterior to parasegment 1 (*e.g.*, those that primarily give rise to the An1, An2, and the anterior majority of Mn) do not seem to organize into precise rows, nor do they exhibit regular division patterns as far as we have observed. Individual segments begin to express *Distal-less-early (Dll-e)* shortly after the onset of *engrailed* expression and, for most segments, *Dll-e* expression is initially restricted to a subset of the daughters of the “d” row, but then expands to include more anterior row progeny that contribute to the developing appendages (Browne et al., 2005; Liubicich et al., 2009). By stage 15, developing limb buds are evident in An1, An2 and Mn, and by stages 23–24 (just prior to cuticle secretion and, as such, the latest stages we can assay by *in situ* hybridization) a full complement of limbs are present and readily distinguished from one another (Fig. 2).

3.3. Head-specific Hox genes (lab, pb, Hox3, and Dfd)

The first Hox genes to be expressed during *Parhyale* embryogenesis are *lab* and *Dfd*. Beginning at stage 8, they are co-expressed in a single, imperfectly aligned row of cells (row 1) prior to grid formation (Fig. 3A-A’). After the onset of *lab* and *Dfd* expression, the ectodermal cells that will form PSPR 2 begin to organize just posterior to row 1 (see progression in Fig. 3A’–D’). Around this same time, cells that will become PSPR 0, just anterior to row 1, begin to weakly express *lab* (Fig. 3B and B’). As *lab* expression levels increase in these cells, they decrease within row 1 (Fig. 3C and C’). By the time that the FMW is initiated in PSPR 2, row 1 typically lacks any detectable *lab* expression—the sole exception to this is the midline cell of row 1, which sometimes remains *lab*-positive during the initial progression of the FMW (Fig. 3D and D’).

When the *lab* and *Dfd* expression domains first become distinct from one another, *Dfd* is strongly expressed in row 1 and *lab* is strongly expressed in two anterior patches on either side of the midline (Fig. 3C and E). There is a one- to two-cell wide (in the A–P direction) region that is composed of cells that express both *lab*

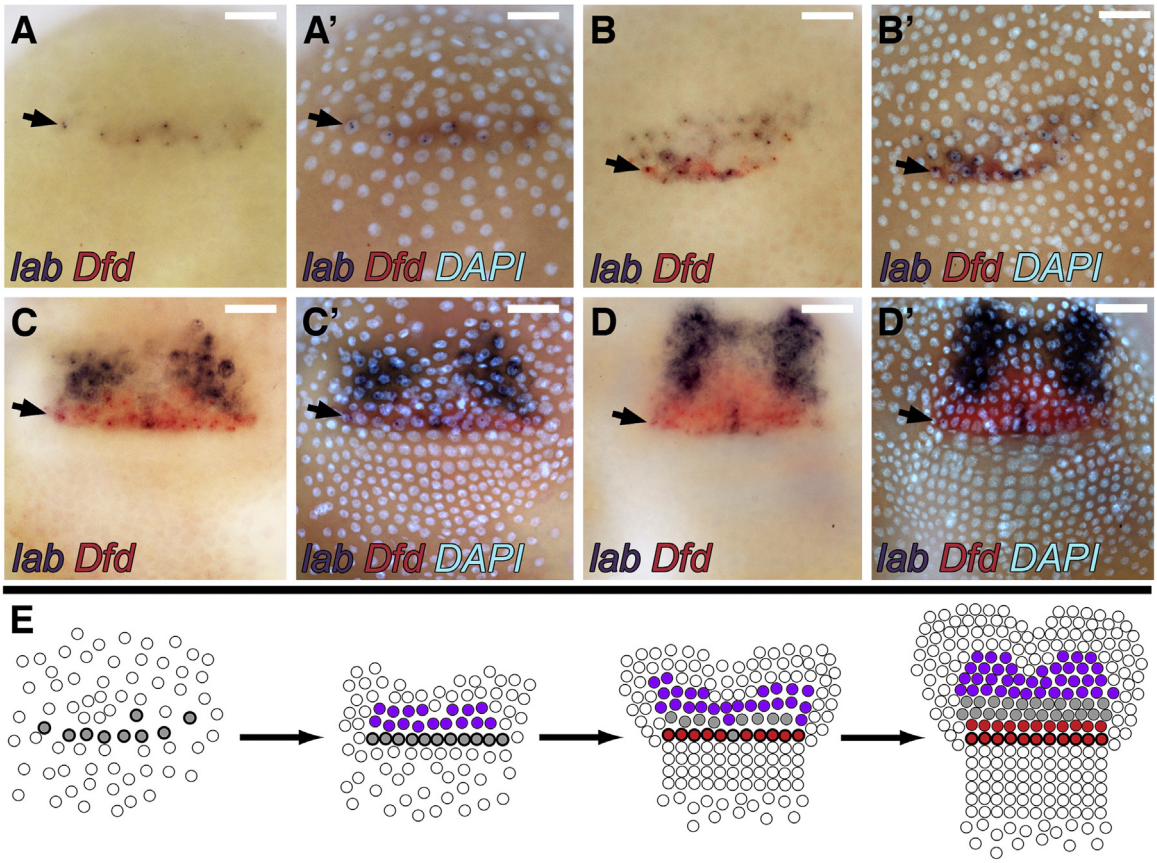

Fig. 3. *lab* and *Dfd* expression during early germband formation and elongation. Anterior is at top. (A–D) Brightfield images of progressively older embryos ranging from stage 8 to 12 following double *in situ* hybridization for *lab* (purple) and *Dfd* (red). Arrows mark row 1 of the developing germband grid. (A'–D') The same four brightfield images shown in A–D, respectively, additionally showing DAPI staining in order to show *lab* and *Dfd* gene expression in relation to the organization of nuclei in the head. (E) Schematic illustration of early *lab* (purple) and *Dfd* (red) expression. Row 1 is shown in bold, and cells that express both *lab* and *Dfd* are colored gray. Scale bars 100 μm in all panels. (For interpretation of the references to color in this figure legend, the reader is referred to the web version of this article.)

and *Dfd*. This co-expression region persists as the exclusively *lab* and *Dfd* expression domains on either side of it begin to expand (Fig. 3D and E). We observe very few cell divisions in this region during this period (based on fixed DAPI preparations and preliminary time-lapse movies), suggesting that the expansion might not be simply due to proliferation of the initial *lab* and *Dfd* expressing cells. This conjecture could be tested in the future with live imaging of GFP tagged versions of these genes.

With the onset of *en1* expression (when it becomes possible to clearly demarcate parasegmental boundaries), it is clear that *Dfd* expression occurs throughout parasegments 0 and 1 (Fig. 4A and B). Segmentally, this corresponds to the very posterior of the An2 segment (in the ventral body region, but not the appendages), the entire Mn segment, and most of M × 1 (with the exception of the *en1*-expressing cells at the very posterior of this segment). By stage 19, as the head appendages are extending, *Dfd* expression in the Mn segment is strongest in the ventral-most region of the segment (where the paragnaths will form) and in the distal tip of the extending mandible, whereas *Dfd* expression throughout the anterior of M × 1 is more uniform (Fig. 4C). At stage 21, this pattern remains relatively unchanged, but there is additional expression in the abdomen, specifically, in the distal regions of the A1-3 appendages (Fig. 4D). By stage 24, *Dfd* expression is localized to the two biramous branches of each developing pleopod (swimmeret) (Fig. 4E). For *lab*, during most of germband elongation, expression levels in An2 are stronger in the lateral regions of the segment, where limb buds will eventually form, than in the ventral region (Fig. 4F). Expression of *lab* can be observed throughout the An2 appendages as they grow, and is also detected at the posterior base of the labrum (Fig. 4G).

The third head-specific Hox gene to be expressed during *Parhyale* embryogenesis is *Hox3*. Its transcripts are first detected around stage 12 in two patches in the head lobes just anterior to the *Dfd* expression domain (Fig. 4H). These *Hox3* domains appear to be predominantly in the posterior half of the future An2 segment, although we also observe *Hox3*-positive cells throughout and immediately posterior to the An2 engrailed stripe (Fig. 4I). Around stage 17, there is a significant decrease in *Hox3* expression anterior to the An2 engrailed stripe (Fig. 4K), such that, by stage 20, *Hox3* is only found in posterior and medial (with regards to the proximal-distal axis) regions of the developing mandibles (Fig. 4J). By stage 24, *Hox3* expression becomes localized to a small patch of mesodermal cells in the mandible (Fig. 2).

Compared to the other three head Hox genes, *pb* comes on relatively late in development. Transcripts are first observed around stage 17 at the anterior base of the second antennae (not shown). This expression domain then extends posteriorly as embryogenesis progresses, such that, by stage 19, *pb* transcripts can be found at the ventral-most base of antenna 2 (Fig. 4L). This staining is still observed through stages 22–24, at which point additional *pb* staining can be detected at the ventral, anterior-most region of the paragnaths of the Mn segment (Figs. 2 and 4M).

3.4. *Hox genes spanning the head and thorax (Scr and Antp)*

Two Hox genes span head and thoracic segments: *Scr* and *Antp*. *Scr* is first expressed around stage 12 in the PSPR 2 cells as they undergo their first round of division to produce the a/b and c/d

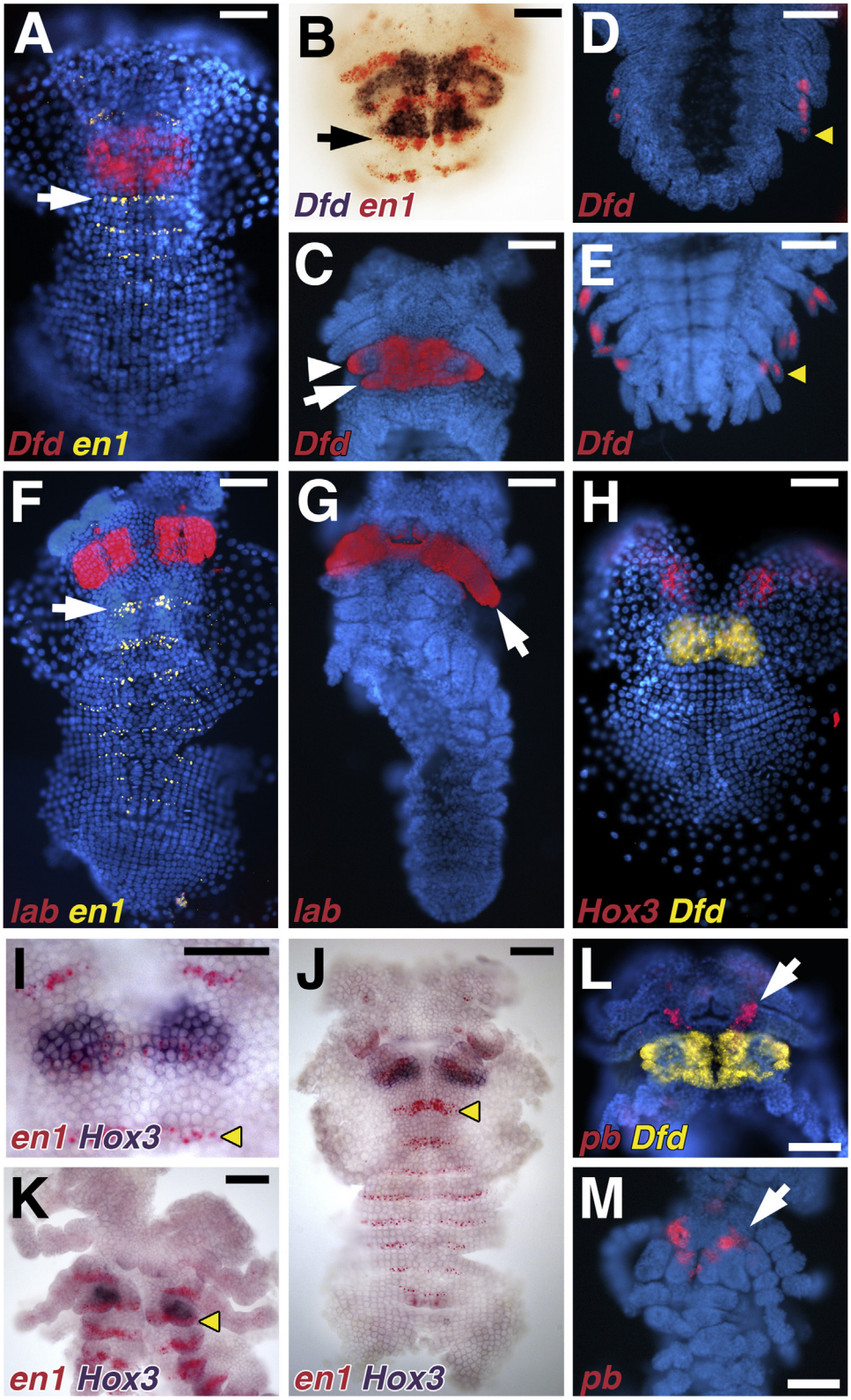

Fig. 4. *Dfd, lab, Hox3* and *pb in situ* hybridization of stage 14–24 embryos. Anterior is at top. A, C–H, and L–M are DAPI stained with *in situ* patterns shown in red or yellow; B and I-K are brightfield images with *in situ* hybridization patterns in purple and red. In panels A, B, F and I–J, *en1* is used as a marker for the posterior boundary of each segment. (A) *Dfd* (red) and *en1* (yellow) expression in a stage 14 embryo. Arrow marks Mx1 *en1* stripe. (B) *Dfd* (purple) and *en1* (red) expression in a stage 17 embryo; arrow marks Mx1 en1 stripe. In this embryo, *Dfd* transcripts are observed throughout parasegments 0 and 1, which corresponds to the posterior of An2 through the anterior of M × 1. (C) *Dfd* (red) expression in a stage 19 embryo. Arrowhead, Mn segment; arrow, M × 1 segment. (D-E) *Dfd* (red) expression in the developing pleopods during stages 21 and 24, respectively. Arrowheads mark the developing A3 pleopod. (F) *lab* (red) and *en1* (yellow) expression in a stage 16 embryo; arrowhead marks Mn *en1* stripe. (G) *lab* (red) expression in An2 (arrow) of a stage 19 embryo. (H) *Hox3* (red) and *Dfd* (yellow) expression in a stage 12 embryo. (I) Close up of *Hox3* (purple) and *en1* (red) expression in a stage 13 embryo; arrowhead marks Mn *en1* stripe. *Hox3* expression is observed in the posterior half of the An2 segment and the anterior-most cells of the Mn segment. (J) *Hox3* expression (purple) is restricted to the developing mandibles in a stage 17 embryo. Expression of *en1* shown in red; arrowhead marks Mn *en1* stripe. (K) *Hox3* (purple) and *en1* (red) expression in a stage 20 embryo; arrowhead marks Mn en1 stripe. (L) *pb* (red) and *Dfd* (yellow) expression in a stage 19 embryo. *pb* is restricted to the base of the An2 appendages (arrow). (M) *pb* expression (red) at the base of the An2 appendages (arrow) and in the paragnaths of a stage 22 embryo. Scale bars 100 μm in all panels. (For interpretation of the references to color in this figure legend, the reader is referred to the web version of this article.)

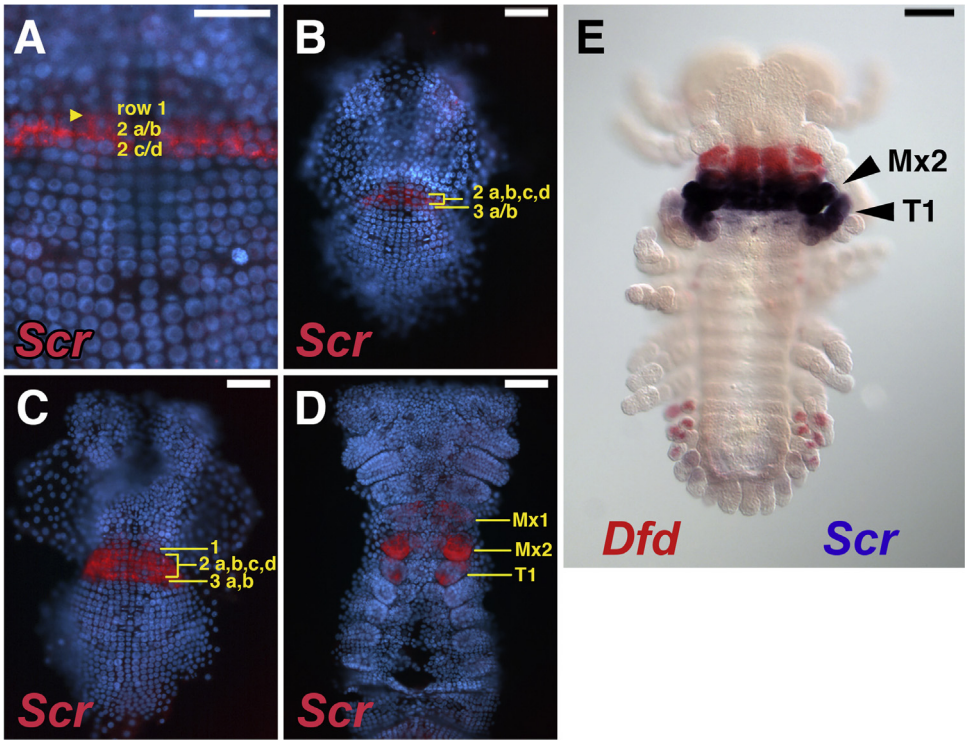

Fig. 5. *Scr in situ* hybridization to stage 12–19 embryos. Anterior is at top. Embryos in A–D are DAPI stained with *in situ* patterns in red. (A) Close up of *Scr* expression in rows 2 a/b and c/d in a stage 12 embryo. Arrowhead: posterior edge of row 1 (B) Stage 14 embryo with *Scr* transcripts in 2 a, b, c, d and 3 a/b. (C) The *Scr* domain expands anteriorly to include cells in parasegment 1 in stage 15 embryos. (D) Stage 19 embryo showing *Scr* expression in M × 1, M × 2 and in the T1 appendage. (E) Stage 24 embryo showing *Dfd* (red) and *Scr* expression (black). *Scr* expression is seen throughout the M × 1 and M × 2 segments and the more distal portions of the T1 appendages. *Dfd* is as far anterior as the Mn segment (expression in more posterior head segments is obscured by the *Scr* signal); expression of *Dfd* is also seen in the A1-A3 pleopods. Scale bars 100 μm in all panels. (For interpretation of the references to color in this figure legend, the reader is referred to the web version of this article.)

daughter rows (Fig. 5A). By stage 15, *Scr* expression expands anteriorly into parasegment 1 and posteriorly into the a and b cells of parasegment 3 (Fig. 5B and C). Together, these cells will give rise to Mx1 through the anterior region of the first thoracic segment (T1). It should be noted that *Scr* expression levels tend to be weaker in Mx1 than in Mx2 throughout development (Figs. 5C, D and 2). During stage 19, as the limb buds begin elongating, *Scr* expression appears more intense in the most distal and proximal regions of the maxillipeds, with only weak or no expression in the medial region, whereas expression throughout the maxillary appendages appear more uniform (Fig. 5D). By stage 23, *Scr* expression is present in both maxillary segments and their appendages, as well as in the T1 appendages (maxilliped), but not the T1 ventral body wall (Fig. 2).

Antp is initially expressed during stage 12 in PSPR 3 cells as they undergo their first division to give rise to a/b and c/d daughter cells (Fig. 6A). The expression boundaries of *Antp* then expand in both the anterior and posterior directions. Anteriorly, in the second parasegment, the c/d cells begin to express *Antp* at stage 13; these cells will eventually be a part of the Mx2 segment (Fig. 6B). At stage 15, the *Antp* expression domain extends from the 2c and d rows through at least parasegment 7 (Fig. 6C). By stage 17–18, *Antp* expression can be found in the very posterior, ventral region of Mx1, throughout all of Mx2 and the developing thoracic segments, and at lower levels in the most ventral (neurogenic) region of the abdominal ectoderm (Fig. 6D). *Antp* expression in Mx2 appears weaker in general than *Antp* expression in the thoracic segments. This expression pattern persists through at least stage 24, the latest time at which we can carry out *in situ* hybridization of whole mount embryos, and the late abdominal *Antp* expression is restricted to the nervous system (Figs. 2 and 6E).

The description provided above for *Antp* transcript distribution in *Parhyale* is based on *in situ* hybridization data, but relating this to where *Antp* functions presents an unusual problem in crustaceans. In at least five previously studies crustacean species, a *Ubx-Antp* bi-cistronic transcript is produced, presumably the result of transcriptional read-through from the *Ubx* promoter (Shiga et al., 2006). In the case of *Daphnia* and *Artemia*, these bi-cistronic transcripts are incapable of generating functional Antp protein (Shiga et al., 2006). Thus, *in situ* probes for *Antp* actually detect the combined expression domains of *Antp* plus *Ubx*. In the case of *Daphnia* and *Artemia*, it was shown that Antp protein was not produced by the bi-cistronic transcripts, and indeed Antp protein was produced in a domain that did not overlap with Ubx.

Parhyale also produces *Ubx-Antp* bi-cistronic transcripts. *Ubx* transcript and protein in *Parhyale* are expressed at moderate levels in T2 and T3, and higher levels from T4-T8 (Liubicich et al., 2009; also summarized below). Therefore, it seemed possible that *Antp* transcripts produced from the *Antp* promoter—*i.e.*, those that make functional Antp protein—are not expressed in the more posterior thoracic segments and appendages, and that the staining observed in this region is solely due to our *Antp* probe hybridizing to *Ubx-Antp* hybrid transcripts. To test this possibility, we used two approaches to detect the distribution of Antp protein. First, we used a previously characterized pair of monoclonal antibodies (MAb 8C11 and MAb 4C3) that have been shown to detect Antp protein across various arthropods (Condie et al., 1991; Hayward et al., 1995; Saenko et al., 2011). Immunostaining reveals that Antp protein is initially broadly expressed in the neurogenic region from Mx2 on posterior, but within the developing appendages, expression is not detected posterior to T3 (Fig. 6F and G). At later stages, the discrepancy between the *in situ* results and antibody staining is even more marked (compare Fig. 6E and H). Antp protein is detected

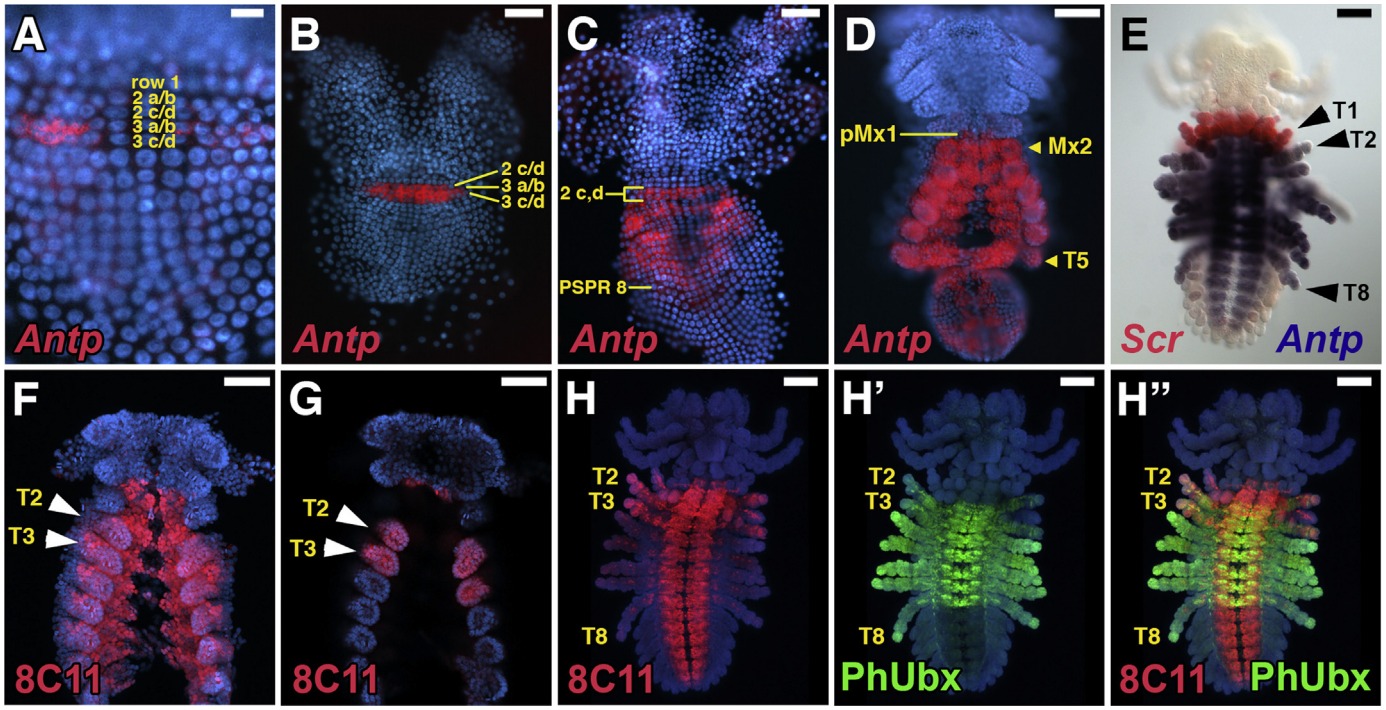

Fig. 6. *Antp in situ* hybridization and immunolocalization. (A) Close up of a stage 12 embryo with *Antp* transcripts accumulating in rows 3 a/b and c/d. (B) *Antp* expression expands anteriorly into 2 c/d by stage 13. (C) Stage 15 embryo displaying *Antp* expression from parasegments 2 through 8. (D) Stage 19 embryo. The most anterior domain of expression is in the CNS in the posterior portion of the Mx1 segment. Expression is rather uniform throughout M × 2 and the entire thorax (thoracic segments posterior to T5 are not visible in this view due to the flexure of the embryo at this stage). Within the abdomen, *Antp* transcripts are expressed in primarily in the neurogenic region. (E) Stage 24 embryo with *Scr* in red and *Antp* in purple. At this stage, *Antp* expression in the head is largely confined to the CNS, is and detectable in the T1 appendage where it overlap with *Scr* expression. (F–G) Immunodetection of Antp proteins with the 8C11 monoclonal antibody suggests post-transcriptional repression in the T4-T8 appendages. (F) Extended focus view of a stage 20 embryos shows expression throughout the thorax in the nervous system and body wall, but (G) optical sections through the developing limbs reveals that Antp protein is not detected in the T4–T8 appendages. (H–H") At stage 24, neuronal expression of Antp (red) is seen from the posterior of the head through to the end of the abdomen. In the appendages and body wall, however, widespread expression is seen in T2 and T3, but in the remaining thoracic appendages, expression is restricted to a small subset of neurons and mesodermal cells. Ubx protein (green) is detected from T2 through T8. Scale bar 20 μm in panel A, 100 μm in panels B–H". (For interpretation of the references to color in this figure legend, the reader is referred to the web version of this article.)

throughout the entirety of the T1–T3 limbs, but restricted to just a small subset of what appear to be neurons and muscle within the developing limbs in T4–T8 (Fig. 6H). Within the nervous system, expression is detected throughout the entire CNS starting at M × 2 (Fig. 6H). Thus, there is overlap of Ubx and Antp protein expression in the CNS, but within the limbs, the two overlap in T2 and T3, but in the remaining thoracic segments, Ubx is expressed throughout the appendages, but Antp is restricted to a small subset of cells (Fig. 6H' and H").

To further confirm the restriction of Antp to the anterior part of the thorax, we used a CRISPR/Cas9 homology mediated knock-in strategy to create embryos in which GFP is inserted in frame with the *Parhyale Antp* coding sequence (see Section 2 and Fig. 7A). This approach yielded GFP- expressing G0 embryos that confirmed the results seen with the 8C11 and 4C3 monoclonal antibodies. Especially striking were late stage embryos (stage 24 and beyond that are stages in which we cannot carry out routine *in situ* or immunohistochemistry due to the cuticle) where we see GFP thoracic appendage expression restricted T1-T3 (Fig. 7B and C). Thus, we are able to conclude that, as in *Daphnia* and *Artemia*, Antp protein does not appear to be expressed from the

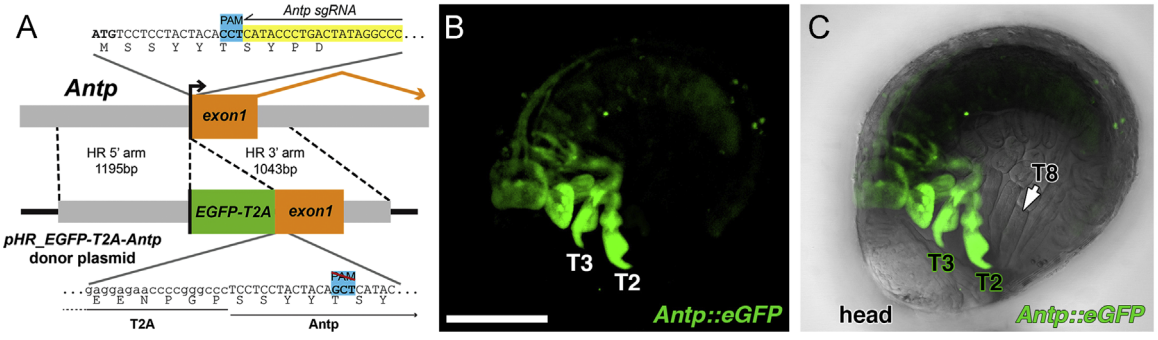

Fig. 7. GFP reporter of Antp *via* CRISPR/Cas9 genome editing. (A) Diagram of the strategy for somatic fluorescent tagging of Antp. A CRISPR gRNA targets the 5′ region of the Antp coding sequence (yellow) and was co-injected with a Cas9 recombinant protein at the one-cell stage. A donor plasmid was provided as a repair template for homologous recombination, generating alleles that incorporate eGFP and the T2A ribosome-skipping site to the N-terminus of the Antp protein. Secondary cleavage of repaired alleles is avoided by a degenerate protospacer-adjacent motif (PAM) sequence (blue). (B, C) Live fluorescent imaging of an eGFP-positive G_0 CRISPR-induced somatic transgenic animal at stage 27. Note the strong signal in T2-T3 limbs, while little signal is seen in the remaining more posterior thoracic limbs. Scale bar 100 μm. (For interpretation of the references to color in this figure legend, the reader is referred to the web version of this article.)

bi-cistronic transcripts in *Parhyale*, and Antp and Ubx overlap less than expected from the *in situ* data.

3.5. Thoracic Hox gene (Ubx)

We previously published a detailed account of *Ubx* transcript and protein expression during *Parhyale* embryogenesis (Liubicich et al., 2009). By stage 23, when *Ubx* expression reaches its full fruition, it is expressed at lower levels in the gnathopods of T2 and T3, and more robustly in the walking legs of T4 through T8 (Figs. 2, 6H', and 8D). There is transient expression of *Ubx* transcripts in the neurogeneic region of the abdomen at stages 17–18, which then resolves to a small subset of neuronal cells before ceasing expression in the abdomen.

3.6. Abdominal Hox genes (abd-A and Abd-B)

The Hox genes that are expressed in the *Parhyale* abdomen are *abd-A* and *Abd-B*. In *Parhyale*, we first detected *abd-A* transcripts at stage 17 in the a/b and c/d cells of parasegments 12 and 13—these cells will eventually give rise to the posterior of A1 through the anterior of A3 (Fig. 8A). At stage 18, we also observe weaker levels of *abd-A* in parasegments 8 through 11, which will go on to form the very posterior of T5 through the anterior of A1. As the limb buds start protruding during stage 19, *abd-A* is expressed strongly in A1-3, more weakly in T6-8, and it is just starting to come on in A4 (Fig. 8B). During stages 21-22, *abd-A* expression appears in the T6-8 appendages, but is absent from the distal most tips, whereas the strong A1-3 and very weak A4 expression appears more homogeneously throughout the limbs (Fig. 8C). By stage 24, we consistently observe *abd-A* expression in the ventral ectoderm from the posterior of T5 through the anterior of A3, and in the appendages of T6 through A3, with very weak staining in the limbs of A4, and no staining in A5, A6 or the telson (Figs. 2 and 8D).

Abd-B is first expressed at stage 17–18 in the b, c, and d cells of parasegment 11, and in the a/b and c/d cells of parasegment 12 (Fig. 8E). By stage 19, *Abd-B* expression remains absent from the T8 en1 stripe, but is present in all of the other cells of parasegment 11, plus the developing parasegments 12, 13 and 14, which together give rise to the anterior of A1 through the anterior of A4 (Fig. 8F). As the germband continues to expand, *Abd-B* is expressed in all of the developing abdominal segments and appendages (Fig. 8G). Finally, at stage 24, *Abd-B* is rather homogeneously expressed throughout the ventral ectoderm from the very posterior of T8 through A6, and in the developing limbs of A1 through A6, but is excluded from the developing telson (Fig. 2).

4. Discussion

Previous studies have examined the expression of subsets of crustacean Hox genes, most notably in the branchiopods *Artemia* and *Daphnia*, the maxillopod *Sacculina*, and in the malacostracans *Porcellio*, *Procambarus* and *Asellus* (Abzhanov and Kaufman, 1999a, 1999b, 2000a, 2000b; Averof and Akam, 1995; Blin et al., 2003; Brena et al., 2005; Copf et al., 2003; Mouchel-Vielh et al., 2002; Papillon and Telford, 2007; Shiga et al., 2002; Vick and Blum, 2010). The work reported here represents the most thorough cloning and expression analysis of Hox genes in a crustacean to date. We have isolated sequences (in most cases, full-length cDNAs) for nine *Parhyale* Hox genes and have shown that at least six of them are linked to other Hox genes in the genome. Further experiments are necessary to determine whether all of these genes lie together in a single cluster, or whether the *Parhyale* Hox complex has been split, as is the case for other arthropod species (Negre and Ruiz, 2007; Yasukochi et al., 2004).

Parhyale has at least eleven distinct appendage types, and each type develops in the presence of a unique set of Hox genes (Fig. 9).

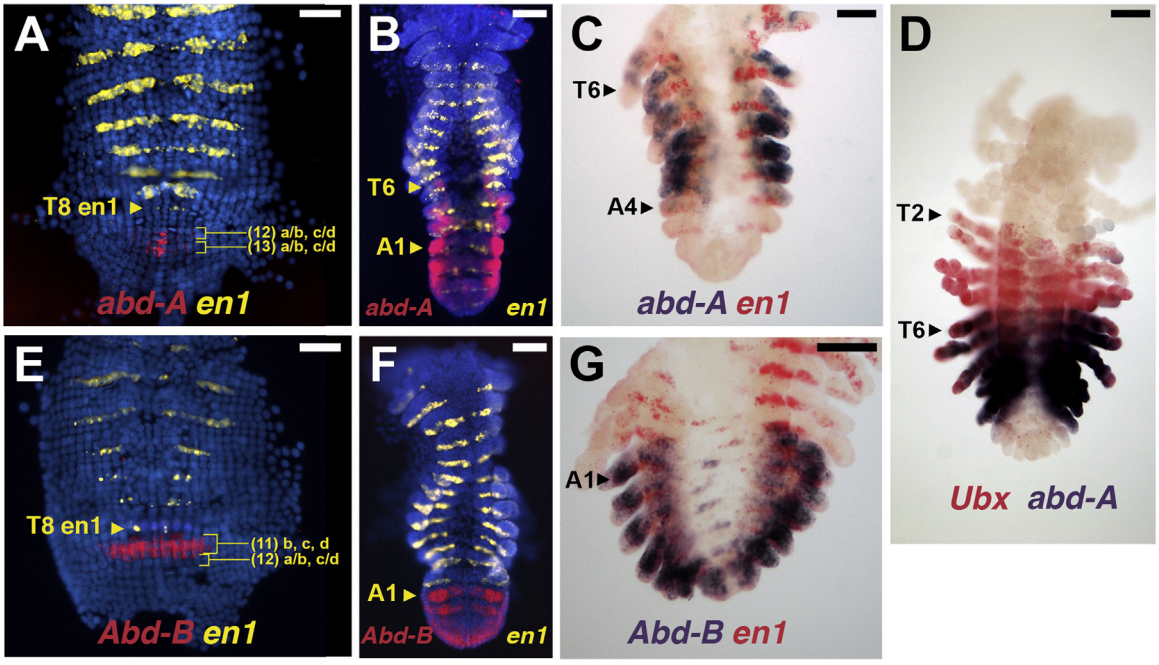

Fig. 8. *abd-A* and *Abd-B in situ* hybridization in stage 17–22 embryos. Anterior is at top. A, B, E and F are DAPI stained with *in situ* patterns in red and yellow; C, D and G are brightfield images with *in situ* hybridization patterns in purple and red. (A) Close up of a stage 17 embryo with *abd-A* expression in developing parasegments 12 and 13; *en1* expression is shown in yellow. (B) *abd-A* (red) and *en1* (yellow) expression in a stage 19 embryo. (C) Stage 21 embryo with *abd-A* expression (purple) at moderate levels in the T6-T8 appendages, at higher levels in the A1–A3 appendages, and at low levels in the A4 appendage; *en1* staining shown in red. (D) Stage 24 embryo with *Ubx* in red and *abdA* in purple. The anterior boundary of *Ubx* is at T2, while *abdA* is expressed thought T6-A3, with low levels in A4. (E) Stage 17 embryo with *Abd-B* transcripts first detectable in rows 11b, c and d, and in 12 a/b and c/d; *en1* expression is shown in yellow. (F) *Abd-B* (red) and *en1* (yellow) expression in a stage 19 embryo. Expression is seen throughout the entire abdomen. (G) Stage 22 embryo with *Abd-B* expression (purple) throughout segments A1-6; *en1* staining shown in red. Scale bars 100 μm in all panels. (For interpretation of the references to color in this figure legend, the reader is referred to the web version of this article.)

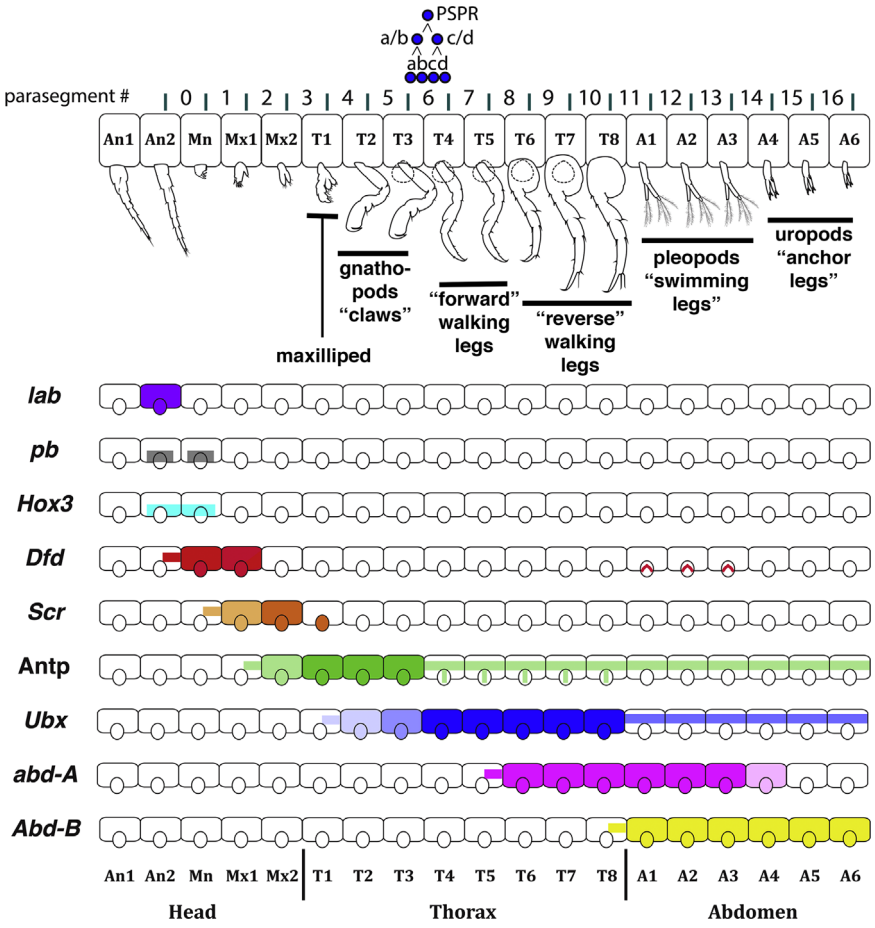

Fig. 9. Summary of Hox gene expression domains in *Parhyale*. At the top is an illustration of the different limb morphologies seen along the *Parhyale* body axis, with an alignment to the numbered Parasegment Precursor Rows (PSPR) and progeny rows (a, b, c, d) that contribute to each segment. Colored bars through the middle of a segment indicate that expression is largely confined to the CNS for these segments (and in the case of *Ubx* the expression in the abdominal CNS is relatively transitory). In many cases, the anterior limit of expression is parasegmental for the CNS, but segmental for the ectoderm and appendages, although in a few cases the anterior CNS domain is transient. The Antp domain shown here represents expression of the protein, as *in situ* hybridization detects the *Antp-Ubx* bi-cistronic message, and bars through the T4-T8 limbs represent expression in a subset of neurons and mesodermal cells in these limbs. For *Ubx*, the CNS expression in the abdomen is transient as shown in Liubicich et al. (2009). For *pb* and *Hox3*, expression occurs within very limited domains that does not include the entire appendage. The chevrons in the A1-3 segments for *Dfd* represent the late patterns seen within these appendages. (For interpretation of the references to color in this figure legend, the reader is referred to the web version of this article.)

For example, as the appendages are developing in the head, the first antenna does not express any Hox genes. The second antenna expresses *lab* and *pb*. For the mandibular (Mn) segment, *Dfd* is expressed throughout the segment, with additional expression of *pb* in the paragnaths and *Hox3* in the mandibles. The first maxillae express both *Dfd* and *Scr*; the second maxillae express *Scr* strongly and *Antp* weakly. Within the anterior thorax *Antp* is the only Hox gene expressed in the T1 body wall, although both *Scr* and *Antp* are strongly expressed in the T1 appendages (maxillipeds), with *Scr* appearing significantly later in embryogenesis; the gnathopods of T2 and T3 are unique in that they express *Antp* plus moderate levels of *Ubx*. High levels of *Ubx* are found in the walking legs of T4–T8, with the posteriorly oriented T6-T8 walking legs additionally expressing *abd-A*. Analysis of Antp protein expression by immunohistochemistry and GFP knock-in reveals that there is initial Antp expression throughout the thorax in the neurogenic region, but expression in the developing appendages is largely restricted to T1-T3, with T4-T8 expression in the limbs restricted to a small subset of cells, most likely neurons and muscle cells. Within the abdomen, the pleopods (swimmerets) of A1-3 express both *abd-A* and *Abd-B*; and *Abd-B* is the only Hox gene expressed at high levels in the uropods of A4-6. Antp protein is expressed in the abdomen, but is restricted to the nervous system. All these patterns are summarized schematically in Fig. 9. These patterns suggest that a complex "Hox code" may be responsible for establishing the morphological differences that exist between these appendage types (Fig. 9). We also note that while the initial expression patterns of the Hox genes follow parasegmental boundaries, and such parasegmental boundaries are maintained for expression in the central nervous system, the expression boundaries in the developing and mature limbs are instead segmental. We previously showed for *Ubx* that the initial parasegmental expression boundary retracted back to a segmental boundary in the ectoderm before limb growth began (Liubicich et al., 2009), and this behavior is also seen here for several of the other Hox genes.

As in many other animals, *Parhyale* Hox genes also exhibit temporal colinearity—that is, those genes located at the proximal or 3′ end of the Hox cluster (*e.g.*, *lab*) are transcribed prior to more distal, 5′ end genes (*e.g.*, *Abd-B*). The only exceptions to this temporal colinearity in *Parhyale* are *pb*, which is located on the proximal end of the Hox cluster but is one of the last Hox genes to be expressed, and *Hox3*, which is first expressed after *Dfd*, but before (or perhaps coincident with) *Scr*.

The only Hox ortholog that we were unable to isolate from *Parhyale* is ftz. Typically, ftz protein sequence, function and expression profiles are highly divergent in arthropods, where they appear to play a role in neurogenesis, segmentation, and/or segment identity depending on the species (Damen, 2002; Heffer

et al., 2010,2013). While we cannot rule out the existence of a *ftz* ortholog in *Parhyale*, our degenerate PCR primers targeted the LELEKEF and KIWFNQR motifs that are conserved in all pancrustaceans (insects and crustaceans) where *ftz* has been isolated (Heffer et al., 2013). Furthermore, genomic sequences obtained from contiguous *Parhyale* BAC clones show that there is no *ftz* between *Scr* and *Antp*, its canonical position in arthropods (Chipman et al., 2014). It is worth mentioning that while *ftz* genes have been isolated from brachiopod and maxillopod crustaceans, no *ftz* ortholog has been reported for any malacostracan crustacean—this includes both *Porcellio* and *Procambarus*, for which numerous Hox genes (including *Scr* and *Antp*) have already been isolated (Abzhanov and Kaufman, 1999a,1999b,2000a,2000b). Whether *ftz* was lost in the entire malacostracan lineage poses an interesting question that awaits further analysis.

The other Hox gene that has diverged significantly during arthropod evolution is *Hox3*. While *Hox3* appears to play a segment identity role in chelicerates and myriapods, in insects (where it is often called *zen*) it typically serves a function in extra-embryonic tissues (Abzhanov and Kaufman, 1999b; Falciani et al., 1996; Hughes and Kaufman, 2002b; Janssen and Damen, 2006; Panfilio et al., 2006; Telford and Thomas, 1998). Prior to this report, only one *Hox3* ortholog had been identified in a crustacean: *Daphnia Hox3*. Its expression pattern, initially expressed in An2 and Mn before ultimately becoming restricted to the mesoderm of the developing mandible (Papillon and Telford, 2007), is strikingly similar to what we observe for *Parhyale Hox3*. Interestingly, *Hox3* is also expressed in the mandibular mesoderm in the centipede *Lithobius* and in *Thermobia,* a member of the early diverging insect lineage Thysanura (Hughes and Kaufman, 2002a; Hughes et al., 2004). It has been suggested that this conserved pattern may have arisen early within Mandibulata, and perhaps may have even played a role in the origin of mandibles (Papillon and Telford, 2007). Our results demonstrate that *Hox3* expression in the mandibular mesoderm also occurs in at least one malacostracan, lending further credence to this hypothesis.

Prior to this work, the isopod *Porcellio* was the only crustacean for which *lab*, *pb* and *Dfd* expression patterns were known (Abzhanov and Kaufman, 1999b). Given that *Porcellio* are isopods (closely related to amphipods), it is not surprising that such expression patterns are similar to, albeit slightly different from, those we observe in *Parhyale*. In both species, *lab* is expressed exclusively in An2 and its appendages, while *pb* is expressed at the base of the second antennae as well as in the paragnaths, a pair of lobes that act as the lower lips of the mandibular apparatus (Wolff and Scholtz, 2006). Both species also exhibit *Dfd* expression in Mn (including the paragnaths and mandibles) and the anterior portion of the Mx1 segment. However, they differ in that *Parhyale Dfd* is additionally expressed in the first maxillae and in the developing swimmerets of A1-A3, while *Porcellio Dfd* is not. To the best of our knowledge, *Parhyale* is the only arthropod for which *Dfd* expression has been observed in abdominal appendages. It will be interesting to examine whether *Dfd* plays a significant role in pleopod development.

Compared to the head-specific Hox genes, *Scr*, *Antp* and *Ubx* have all received considerably more attention in crustaceans. *Ubx* expression is typically restricted to the thorax, and its anterior boundary marks the transition between feeding appendages (*e.g.*, maxillae or maxillipeds) and locomotory appendages (Averof and Patel, 1997). Our previously published expression and functional data on *Parhyale Ubx* confirms that this gene plays a role in specifying this transition (Liubicich et al., 2009; Pavlopoulos et al., 2009).

The expression patterns associated with *Scr* have been previously examined in two malacostracan crustaceans: *Porcellio* (which, like *Parhyale*, has a single pair of maxillipeds on T1) and the crayfish *Procambarus* (which have three pairs of maxillipeds located on segments T1-T3). In *Porcellio*, *Scr* transcripts are expressed in Mx1 and Mx2 segments and their appendages, and in the T1 maxilliped (Abzhanov and Kaufman, 1999a); these expression boundaries coincide with what we see in *Parhyale*. The *Procambarus Scr* pattern is similar to this except for the absence of *Scr* transcripts in Mx1 (Abzhanov and Kaufman, 2000a). In both *Porcellio* and *Procambarus*, Scr protein is detected early in second maxillae, but comes on much later in the T1 maxilliped, presumably as a result of post-transcriptional regulation (Abzhanov and Kaufman, 1999a). Whether a similar post-transcriptional regulation of Scr protein occurs in *Parhyale* awaits future experiments.

Our *in situ* hybridization experiments using probes for *Parhyale Antp* reveal a pattern similar to that reported for *Porcellio Antp* in that both are observed in Mx2 through most of the thorax, with additional staining in the abdominal neuroectoderm and CNS. A similar pattern of *Antp* mRNA expression (*i.e.*, from Mx2 through most or all of the thorax) has been observed in the branchiopods *Artemia* and *Daphnia*, and during the early stages of *Procambarus* development (Abzhanov and Kaufman, 2000a; Averof and Akam, 1995; Shiga et al., 2002). However, it has been shown that all of these species produce *Ubx-Antp* read-through transcripts, and in at least two of these species (*Artemia* and *Daphnia*), Antp protein is not translated from these chimeric transcripts (Shiga et al., 2002, 2006); we find the same appears to be true in *Parhyale*. This suggests that the previously described posterior boundaries for *Antp* expression (*i.e.*, at the border between the thorax and abdomen) may merely reflect transcription of the *Ubx-Antp* read-through transcripts from the *Ubx* promoter(s) rather than bona fide *Antp* expression. Consistent with this, Antp protein expression has been found to be more anteriorly restricted in several of these species than the initial *in situ* hybridization analyses suggested. For example, Antp protein is only expressed in Mx1 in *Artemia*, and in Mx1 and T1 of *Daphnia* (Shiga et al., 2002, 2006). Furthermore, during later stages in *Procambarus*, *Antp* transcripts are restricted to Mx1 through T3, suggesting that no *Ubx-Antp* read-through transcripts are being produced at this late stage (Abzhanov and Kaufman, 2000a). Intriguingly, in all three of these cases, *Antp*-specific transcripts and/or Antp protein are only found in Mx2 and in those thoracic appendages that do not express Ubx protein, or, in the case of *Parhyale*, express Ubx at lower levels than the rest of the thorax. This raises the possibility that *Ubx* may negatively regulate *Antp* in these species, perhaps by acting as a transcriptional repressor of the *Antp* promoter as it does in *Drosophila* (Beachy et al., 1988). Alternatively, the production of *Ubx-Antp* readthrough transcripts might somehow physically interfere with the transcription of *Antp*-specific transcripts from the *Antp* promoter in these species.

We found that *Parhyale abd-A* is expressed in T6–8 and A1–A3, and is detected at very low levels in A4. This general pattern of being expressed in the posterior-most thoracic segments and the anterior-most abdominal segments has also been observed in the three other malacostracans for which *abd-A* expression has been examined: *Asellus, Porcellio* and *Procambarus. In situ* hybridizations for *Asellus abd-A* revealed staining in T6-T8, in A1-A2, but not in A3-A6 (Vick and Blum, 2010). *Porcellio abd-A* has three splicing variants: *abd-A1* and *abd-A2* are expressed in a graded manner (stronger in anterior, weaker toward the posterior) in A1-5, but not A6. *abd-A3* also shows a graded expression pattern in A1-A5, with additional expression in T6–T8 (Abzhanov and Kaufman, 2000b). *Procambarus abd-A* is similarly expressed in A1-A5, and shows additional expression in the appendages of T7 and T8 (Abzhanov and Kaufman, 2000a). The authors suggested that *abd-A* may play two roles in *Procambarus*, namely, specifying abdominal identity and differentiating posterior thoracic appendages from more anterior ones. Consistent with this idea, in *Parhyale*, the

abd-A expressing walking legs (T6-T8) differ significantly in morphology from their more anterior counterparts (T4–T5)—they are larger, have thicker bristles, and are positioned in the opposite orientation (*i.e.*, curved posteriorly rather than anteriorly).

There also appears to be a correlation between *abd-A* expression and morphological differences in the abdomen. For instance, in *Asellus, abd-A* is expressed in the two free abdominal segments (A1–A2), but not in the pleotelson, a structure specific to some groups of isopods and comprised of A3-6 fused with the telson (Vick and Blum, 2010). In both *Porcellio* and *Procambarus, abd-A* is expressed in A1–A5, which give rise to pleopods (swimmerets), but not in A6, which gives rise to a single pair of uropods. *Parhyale* and other amphipods have a different arrangement of abdominal appendages: they bear pleopods on A1-A3 and uropods on A4-A6. Intriguingly, *Parhyale abd-A* is expressed strongly in the pleopod-bearing segments (A1-A3), and either very weakly or not at all in the uropod-bearing segments (A4–A6). This raises the possibility that, in malacostracans, evolutionary changes in the posterior boundary of *abd-A* have facilitated morphological diversity in abdominal appendage type (*e.g.*, number of pleopods versus uropods) in a manner similar to how changes in the anterior boundary of *Ubx* lead to diversity in thoracic appendage type (*e.g.*, number of maxillipeds versus walking legs) (Averof and Patel, 1997; Liubicich et al., 2009; Pavlopoulos et al., 2009).

To date, *Abd-B* expression has only been examined in two malacostracans, *Porcellio* and *Parhyale*, and in both cases, it is expressed in all abdominal segments and their appendages (Brena et al., 2005; this work). This suggests that *Abd-B* may be involved in specifying abdominal identity in these species. A hallmark feature of malacostracan abdominal appendages (*i.e.*, pleopods and uropods) is their biramous nature. It will be interesting to determine whether *Abd-B* plays a role in directing biramous appendage development, and/or in specifying uropod identity (as *Abd-B* is the only Hox gene expressed in the uropods of *Porcellio* and *Parhyale*).

In summary, our analysis provides the most complete picture to date of Hox gene expression in a crustacean. Hox gene expression in *Parhyale* generally follows the properties of spatial and temporal colinearity, with a complex pattern of overlapping domains that suggests a “Hox code” that may specify the eleven distinct appendage types observed in *Parhyale*. Given that techniques for gene misexpression and knock down have already been established in *Parhyale*, these and other questions regarding Hox gene function, and the role of Hox genes in generating the diverse arrangements of crustacean body plans, can be addressed in future experiments in this emerging model organism.

Acknowledgments

We thank Ron Parchem for the *Parhyale en1* clone, Jay Rehm for thoughtful discussions regarding early germband cell divisions in *Parhyale*, Rachel Thayer for the *abd-A in situ* in Fig. 2, and Rob White for providing the FP6.87 monoclonal antibody. The BAC sequencing work conducted by the U.S. Department of Energy Joint Genome Institute was supported by the Office of Science of the U.S. Department of Energy under Contract no. DE-AC02-05CH11231. This work was supported by NSF Grant IOS-1257379 to NHP.

Appendix A. Supplementary material

Supplementary data associated with this article can be found in the online version at http://dx.doi.org/10.1016/j.ydbio.2015.10.029.

References

Abzhanov, A., Kaufman, T.C., 1999a. Novel regulation of the homeotic gene Scr associated with a crustacean leg-to-maxilliped appendage transformation. Development 126, 1121–1128.
Abzhanov, A., Kaufman, T.C., 1999b. Homeotic genes and the arthropod head: expression patterns of the labial, proboscipedia, and Deformed genes in crustaceans and insects. Proc. Natl. Acad. Sci. 96, 10224–10229.
Abzhanov, A., Kaufman, T.C., 2000a. Embryonic expression patterns of the Hox genes of the crayfish Procambarus clarkii (Crustacea, Decapoda). Evol. Dev. 2, 271–283.
Abzhanov, A., Kaufman, T.C., 2000b. Crustacean (malacostracan) Hox genes and the evolution of the arthropod trunk. Development 127, 2239–2249.
Angelini, D.R., Kaufman, T.C., 2005. Insect appendages and comparative ontogenetics. Dev. Biol. 286, 57–77.
Averof, M., Akam, M., 1995. Hox genes and the diversification of insect and crustacean body plans. Nature 376, 420–423.
Averof, M., Patel, N.H., 1997. Crustacean appendage evolution associated with changes in Hox gene expression. Nature 388, 682–686.
Bassett, A., Liu, J.-L., 2014. CRISPR/Cas9 mediated genome engineering in Drosophila. Methods 69, 128–136.
Beachy, P.A., Krasnow, M.A., Gavis, E.R., Hogness, D.S., 1988. An Ultrabithorax protein binds sequences near its own and the Antennapedia P1 promoters. Cell 55, 1069–1081.
Blin, M., Rabet, N., Deutsch, J.S., Mouchel-Vielh, E., 2003. Possible implication of Hox genes Abdominal-B and abdominal-A in the specification of genital and abdominal segments in cirripedes. Dev. Genes. Evol. 213, 90–96.
Brena, C., Liu, P.Z., Minelli, A., Kaufman, T.C., 2005. Abd-B expression in Porcellio scaber Latreille, 1804 (Isopoda: Crustacea): conserved pattern versus novel roles in development and evolution. Evol. Dev. 7, 42–50.
Browne, W.E., Price, A.L., Gerberding, M., Patel, N.H., 2005. Stages of embryonic development in the amphipod crustacean, Parhyale hawaiensis. Genesis 42, 124–149.
Chipman, A.D., Ferrier, D.E.K., Brena, C., Qu, J., Hughes, D.S.T., Schröder, R., Torres-Oliva, M., Znassi, N., Jiang, H., Almeida, F.C., et al., 2014. The first myriapod genome sequence reveals conservative arthroEpod gene content and genome organisation in the centipede Strigamia maritima. Plos Biol. 12, e1002005.
Condie, J.M., Mustard, J.A., Brower, D.L., 1991. Generation of anti-Antennapedia monoclonal antibodies and Antennapedia protein expression in imaginal discs. Dros Inf. Serv. 70, 52–54.
Copf, T., Rabet, N., Celniker, S.E., Averof, M., 2003. Posterior patterning genes and the identification of a unique body region in the brine shrimp Artemia franciscana. Development 130, 5915–5927.
Damen, W.G., 2002. Fushi tarazu: a Hox gene changes its role. BioEssays 24, 992–995.
Diao, F., White, B.H., 2012. A novel approach for directing transgene expression in Drosophila: T2A-Gal4 in-frame fusion. Genetics 190, 1139–1144.
Falciani, F., Hausdorf, B., Schröder, R., Akam, M., Tautz, D., Denell, R., Brown, S., 1996. Class 3 Hox genes in insects and the origin of zen. Proc. Natl. Acad. Sci. 93, 8479–8484.
Hayward, D.C., Patel, N.H., Rehm, E.J., Goodman, C.S., Ball, E.E., 1995. Sequence and Expression of Grasshopper Antennapedia: Comparison to Drosophila. Dev. Biol. 172, 452–465.
Heffer, A., Shultz, J.W., Pick, L., 2010. Surprising flexibility in a conserved Hox transcription factor over 550 million years of evolution. Proc. Natl. Acad. Sci. 107, 18040–18045.
Heffer, A., Xiang, J., Pick, L., 2013. Variation and constraint in Hox gene evolution. Proc. Natl. Acad. Sci. 110, 2211–2216.
Hughes, C.L., Kaufman, T.C., 2002a. Hox genes and the evolution of the arthropod body plan. Evol. Dev. 4, 459–499.
Hughes, C.L., Kaufman, T.C., 2002b. Exploring the myriapod body plan: expression patterns of the ten Hox genes in a centipede. Development 129, 1225–1238.
Hughes, C.L., Liu, P.Z., Kaufman, T.C., 2004. Expression patterns of the rogue Hox genes Hox3/zen and fushi tarazu in the apterygote insect Thermobia domestica. Evol. Dev. 6, 393–401.
Janssen, R., Budd, G.E., 2010. Gene expression suggests conserved aspects of Hox gene regulation in arthropods and provides additional support for monophyletic Myriapoda. EvoDevo 1, 4.
Janssen, R., Damen, W.G., 2006. The ten Hox genes of the millipede Glomeris marginata. Dev. Genes Evol. 216, 451–465.
Liubicich, D.M., Serano, J.M., Pavlopoulos, A., Kontarakis, Z., Protas, M.E., Kwan, E., Chatterjee, S., Tran, K.D., Averof, M., Patel, N.H., 2009. Knockdown of Parhyale Ultrabithorax recapitulates evolutionary changes in crustacean appendage morphology. Proc. Natl. Acad. Sci. 106, 13892–13896.
Mahfooz, N.S., Li, H., Popadić, A., 2004. Differential expression patterns of the hox gene are associated with differential growth of insect hind legs. Proc. Natl. Acad. Sci. A 101, 4877–4882.
Misof, B., Liu, S., Meusemann, K., Peters, R.S., Donath, A., Mayer, C., Frandsen, P.B., Ware, J., Flouri, T., Beutel, R.G., 2014. Phylogenomics resolves the timing and pattern of insect evolution. Science 346, 763–767.
Mouchel-Vielh, E., Blin, M., Rigolot, C., Deutsch, J.S., 2002. Expression of a homologue of the fushi tarazu (ftz) gene in a cirripede crustacean. Evol. Dev. 4, 76–85.
Negre, B., Ruiz, A., 2007. HOM-C evolution in Drosophila: is there a need for Hox gene clustering? Trends Genet. 23, 55–59.

Panfilio, K.A., Liu, P.Z., Akam, M., Kaufman, T.C., 2006. Oncopeltus fasciatus zen is essential for serosal tissue function in katatrepsis. Dev. Biol. 292, 226–243.
Papillon, D., Telford, M.J., 2007. Evolution of Hox3 and ftz in arthropods: insights from the crustacean Daphnia pulex. Dev. Genes. Evol. 217, 315–322.
Parchem, R.J., Poulin, F., Stuart, A.B., Amemiya, C.T., Patel, N.H., 2010. BAC library for the amphipod crustacean,Parhyale hawaiensis. Genomics 95, 261–267.
Patel, N.H., 1994. Imaging neuronal subsets and other cell types in whole-mount Drosophila embryos and larvae using antibody probes. Methods Cell. Biol. 44, 445–487.
Patel, N.H., Kornberg, T.B., Goodman, C.S., 1989. Expression of engrailed during segmentation in grasshopper and crayfish. Development 107, 201–212.
Pavlopoulos, A., Kontarakis, Z., Liubicich, D.M., Serano, J.M., Akam, M., Patel, N.H., Averof, M., 2009. Probing the evolution of appendage specialization by Hox gene misexpression in an emerging model crustacean. Proc. Natl. Acad. Sci. 106, 13897–13902.
Peterson, M.D., Rogers, B.T., Popadić, A., Kaufman, T.C., 1999. The embryonic expression pattern of labial, posterior homeotic complex genes and the teashirt homologue in an apterygote insect. Dev. Genes Evol. 209, 77–90.
Pourquié, O., 2009. Hox genes. Elsevier Academic Press, San Diego.
Price, A.L., Patel, N.H., 2008. Investigating divergent mechanisms of mesoderm development in arthropods: the expression of Ph-twist and Ph-mef2 in Parhyale hawaiensis. J. Exp. Zool. B Mol. Dev. Evol. 310, 24–40.
Regier, J.C., Shultz, J.W., Zwick, A., Hussey, A., Ball, B., Wetzer, R., Martin, J.W., Cunningham, C.W., 2010. Arthropod relationships revealed by phylogenomic analysis of nuclear protein-coding sequences. Nature 463, 1079–1083.
Rehm, E.J., Hannibal, R.L., Chaw, R.C., Vargas-Vila, M.A., Patel, N.H., 2009a. The crustacean Parhyale hawaiensis: a new model for arthropod development. Cold Spring Harb. Protoc, pdb.emo. 114.
Rehm, E.J., Hannibal, R.L., Chaw, R.C., Vargas-Vila, M.A., Patel, N.H., 2009b. In situ hybridization of labeled RNA probes to fixed Parhyale hawaiensis embryos. Cold Spring Harb. Protoc., pdb.prot5130
Rehm, E.J., Hannibal, R.L., Chaw, R.C., Vargas-Vila, M.A., Patel, N.H., 2009c. Fixation and dissection of Parhyale hawaiensis embryos. Cold Spring Harb. Protoc., pdb.prot5127
Rehm, E.J., Hannibal, R.L., Chaw, R.C., Vargas-Vila, M.A., Patel, N.H., 2009d. Antibody staining of Parhyale hawaiensis embryos. Cold Spring Harb. Protoc., pdb.prot5129
Rogers, B.T., Peterson, M.D., Kaufman, T.C., 1997. Evolution of the insect body plan as revealed by the Sex combs reduced expression pattern. Development 124, 149–157.
Saenko, S.V., Marialva, M.S., Beldade, P., 2011. Involvement of the conserved Hox gene Antennapedia in the development and evolution of a novel trait. EvoDevo 2, 1–10.
Shiga, Y., Yasumoto, R., Yamagata, H., Hayashi, S., 2002. Evolving role of Antennapedia protein in arthropod limb patterning. Development 129, 3555–3561.
Shiga, Y., Sagawa, K., Takai, R., Sakaguchi, H., Yamagata, H., Hayashi, S., 2006. Transcriptional readthrough of Hox genes Ubx and Antp and their divergent post-transcriptional control during crustacean evolution. Evol. Dev. 8, 407–414.
Telford, M.J., Thomas, R.H., 1998. Of mites and zen: expression studies in a chelicerate arthropod confirm zen is a divergent Hox gene. Dev. Genes Evol. 208, 591–594.
Vargas-Vila, M.A., Hannibal, R.L., Parchem, R.J., Liu, P.Z., Patel, N.H., 2010. A prominent requirement for single-minded and the ventral midline in patterning the dorsoventral axis of the crustacean Parhyale hawaiensis. Development 137, 3469–3476.
Vick, P., Blum, M., 2010. The isopod Asellus aquaticus: a novel arthropod model organism to study evolution of segment identity and patterning. Palaeodiversity 3, 89–97.
Wolff, C., Scholtz, G., 2006. Cell lineage analysis of the mandibular segment of the amphipod Orchestia cavimana reveals that the crustacean paragnaths are sternal outgrowths and not limbs. Front. Zool. 3, 19.
Yasukochi, Y., Ashakumary, L.A., Wu, C., Yoshido, A., Nohata, J., Mita, K., Sahara, K., 2004. Organization of the Hox gene cluster of the silkworm, Bombyx mori: a split of the Hox cluster in a non-Drosophila insect. Dev. Genes Evol. 214, 606–614.